Table 1
Summary of *in vitro* micronucleus tests.

Chemical	Solvent	Dose (μg/mL)	S9 mix	Cytotoxicity (relative cell survival) (%)	MN frequency (%)[b]	Control MN frequency (%)[b]
EMS	PBS	1000	–	101.0	10.15[c]	1.65[c]
MNNG	DMSO	2	–	98.5	13.25[c]	1.90[c]
PhIP	DMSO	12	+	79.5	16.00[c]	0.75[c]
B[*a*]P	DMSO	10	+	52.5	11.00[c]	1.25[c]
DMBA	DMSO	3	+	69.5	17.50[c]	0.75[c]
4-NQO	DMSO	0.5	–	62.1	5.90[c]	0.70[c]
Caffeine	DW	2000	–	92.7	4.35[c]	0.60[c]
Maltol	Saline	200	–	69.3	4.75[c]	0.55[c]
NaCl	MEM[a]	7500	–	85.2	4.00[c]	0.75[c]

[a] Culture medium (MEM supplemented with 10% CS).
[b] Mean of duplicate culture.
[c] $p < 0.001$ vs. controls by Fisher's exact test.

conducted to confirm reproducibility. The peak area was calculated using Masslynx version 4.0 (Waters) and normalized using the peak areas of dG and the internal standard (I.S.) as described by the following equation: Normalized peak area = (peak area of putative DNA adducts)/(dG area)/(I.S. area) × 10^7.

3. Results

3.1. Induction of micronucleated (MN) cells

The results from *in vitro* micronucleus tests with CHL/IU cells are summarized in Table 1. Since all test compounds are known to induce MN cells with various MOA in the presence or absence of S9-mix, the appropriate experimental conditions were determined in the present experiments. All test compounds induced significantly higher MN incidences (>4.0%) than the corresponding controls (solvents) at the concentrations giving higher than 50% cell survival. The incidence of MN cells in the negative control (solvent) ranged from 0.7 to 1.9%. The carcinogens, PhIP, B[*a*]P, and DMBA, significantly induced MN in the presence of S9-mix ($p < 0.001$), whereas other carcinogens, EMS, MNNG, and 4-NQO, and non-carcinogens, caffeine, maltol, and sodium chloride, induced MN in the absence of S9-mix ($p < 0.001$). These treatment conditions were used for the subsequent comprehensive DNA adductome analysis.

3.2. DNA adductome analysis

In the LC–MS/MS chromatograms of all samples derived from the cells treated with the 6 test carcinogens (groups A and B), putative DNA adduct peaks were detected. The detected peak molecular ion (*m/z*), retention times, normalized peak areas, and identified or presumed DNA adducts obtained from the chromatograms are summarized in Table 2. Among the test carcinogens, most adduct peaks were detected by both digestion methods; however, the PhIP-8-dG adduct was detected only by the nuclease P1 method, and the B[*a*]P and DMBA-induced DNA adducts were detected only by the MCN/SPD method. Non-carcinogens(group C) yielded no DNA adduct peaks, even under the conditions that showed positive results in the MN tests. The possible structures of some DNA adducts were estimated from their *m/z* according to the findings of previous reports (Fig. 2).

A representative chromatogram of *N*-methyl-*N*′-nitro-*N*-nitrosoguanidine (MNNG)-treated samples is shown in Fig. S1. Two peaks at *m/z* 282 corresponding to the molecular ion of methylated dG were detected in the MNNG-treated samples. The first peak (retention time: 7.6 min) was identified as N^7-methyl-2′-deoxyguanosine (N^7-methyl-dG), and the second peak (retention time: 13.7 min) was identified as O^6-methyl-2′-deoxyguanosine (O^6-methyl-dG) by comparison with the chromatograms of each standard substance.

For ethylmethanesulfonate (EMS), two peaks at *m/z* 296 were detected (Fig. S2), and the molecular ion corresponded to ethylated dG. The first and second peaks were thought to be N^7-ethyl-2′-deoxyguanosine (N^7-ethyl-dG) and O^6-ethyl-2′deoxyguanosine (O^6-ethyl-dG), respectively, because the amount and polarity of N^7-ethyl-dG would be higher than those of O^6-ethyl-dG [6].

For 2-amino-6-phenyl-1-methylimidazo[4,5-b]pyrene (PhIP), the peaks at *m/z* 450 and 490 were detected (Figs. S3 and S4), and the *m/z* 490 corresponded to *N*-(deoxyguanosin-8-yl)-PhIP (PhIP-8-dG).

For benzo[*a*]pyrene (B[*a*]P), two peaks at *m/z* 570 were detected (Fig. S5). These peaks were considered to be 10-(deoxyguanosine-N^2-yl)-7,8,9-trihydroxy-7,8,9,10-tetrahydrobenzo[*a*]pyrene (B[*a*]P-DE-N^2-dG).

For 7,12-dimethylbenz[*a*]anthracene (DMBA), 12 possible DNA adducts were detected (Figs. S6–S12).

For 4-nitroquinoline-1-oxide (4-NQO), several peaks were detected (Fig. S13–S16). The *m/z* 410 corresponded to 3-(deoxyadenosin-N^6-yl)-4-aminoquinoline 1-oxide (4-AQO-N^6-dA), and *m/z* 426 corresponded to 3-(deoxyguanosine-N^2-yl)-4-aminoquinoline 1-oxide (4-AQO-N^2-dG) and *N*-(deoxyguanosine-8-yl)-4-aminoquinoline 1-oxide (4-AQO-8-dG).

All adduct peaks with their *m/z*, retention times, and peak areas are illustrated in the adductome maps (Fig. 3).

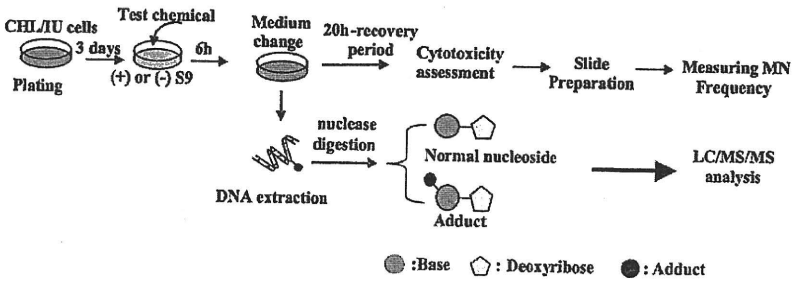

Fig. 1. Schematic outline of the *in vitro* MN test and adductome analysis.

Table 2
Summary of adductome analysis.

Group	Chemical	Peak no.	*m/z*	RT (min)	Normalized peak area		Identified or presumed adducts
					MCN/SPD method	NucleaseP1 method	
A	MNNG	1	282	7.6	2163	2240	N^7-methyl-dG*
		2		13.7	157	158	O^6-methyl-dG*
	EMS	1	296	9.6	2994	5816	N^7-ethyl-dG
		2		16.0	33	235	O^6-ethyl-dG
B	PhIP	1	450	19.1	N.D.	5	–
		2	490	19.6	N.D.	16	PhIP-dG
	B[*a*]P	1	570	22.1	2	N.D.	B[*a*]P-DE-N^2-dG
		2		22.5	6	N.D.	
	DMBA	1	558	24.6	3	N.D.	DMBA-DE-dA
		2	572	19.3	8	N.D.	–
		3		21.4	10	N.D.	–
		4	574	19.3	5	N.D.	DMBA-DE-dG
		5		22S.7	13	N.D.	
		6		23.5	25	N.D.	
		7	590	17.6	12	N.D.	–
		8		18.1	17	N.D.	
		9	596	23.5	5	N.D.	Sodium adducts of No.6
		10	606	18.7	14	N.D.	–
		11		20.7	3	N.D.	–
		12	612	19.3	4	N.D.	–
	4NQO	1	371	14.2	7	4	–
		2	410	12.3	155	112	4-AQO-N^6-dA
		3		17.3	N.D.	6	
		4	426	14.2	4	3	4-AQO-N^2-dG or 4-AQO-8-dG
		5		14.7	4	24	
		6	456	14.6	4	12	–
C	Caffeine Maltol NaCl	No specific peak was detected					

"N.D." means "not detected". "–" represents unknown adduct.
Adducts with and without asterisk show "identified" and "presumed" adducts, respectively.

4. Discussion

In this study, we used the adductome approach to detect the DNA damage caused by the compounds that gave positive results in the MN test condition. Three categories of compounds with different MOA for MN induction were selected. All tested carcinogens were confirmed to form DNA adducts; in contrast, three non-carcinogens yielded no DNA adduct peaks.

In the group A compounds consisting of DNA alkylating agents, O^6- and N^7-methyl-dG and O^6- and N^7-ethyl-dG were detected in the MNNG- and EMS-treated cells, respectively. Although N^3-methyl-dA and N^3-ethyl-dG have been found in other chromatographic analyses [6,7], these adducts were not detected in this adductome analysis, which was probably due to their instability. Another minor lesion, 1-methyl dG, was not detected because its amount was considered to be lower than the detection limit. These results indicate that alkylation of O^6 and N^7 positions of dG would be proof of DNA damage by the group A compounds in the MN-positive experimental condition.

In the group B compounds producing DNA bulky adducts, each compound yielded at least two DNA adduct peaks in the adductome analysis. PhIP yielded two peaks at *m/z* 450 and 490; the former peak is one of unidentified minor adducts [8], but the latter peak is coincident with PhIP-8-dG, the major adduct formed through a reactive intermediate *N*-acetoxy-PhIP [8]. B[*a*]P yielded two peaks at *m/z* 570, which are coincident with the molecular ions of the major adducts B[*a*]P-DE-N^2-dG consisting of four types of stereoisomers [9]. DMBA yielded twelve possible adduct peaks, which agrees with the report showing at least eight DNA adducts induced by DMBA with the ^{32}P-post-labeling analysis [11]. Three DMBA-induced peaks at *m/z* 574 would be stereoisomers of the DMBA-dG adduct, and a peak at *m/z* 558 is coincident with the molecular ion of DMBA-dA, but other peaks are unknown adducts. Six possible DNA adduct peaks were detected in the 4-NQO-treated cellular DNA. Two peaks at *m/z* 410 and 426 correspond to 4-AQO-dG and 4-AQO-dA adducts, respectively, in which several types of 4-NQO binding to C8, N^2, and N^6 of dG and dA are included [12–15], and other peaks cannot be identified because 4-NQO produces various base lesions with different half-life periods [16,17]. These results indicate that the adductome analysis can detect various types of DNA bulky adducts that were identified with the existing methods by other investigators. The efficiency of the adduct peak detection is different between nuclease P1 and MCN/SPD digestion methods in each compound because their enzyme activities on adducted-base excision would vary dependent on the adduct structures. The use of both digestion methods is necessary to detect DNA adducts when new chemicals are tested.

None of the group C compounds, caffeine, maltol, and sodium chloride, which are non-carcinogens but known to produce MN, yielded adduct peaks. Caffeine may interact with DNA repair enzymes and/or nucleotide precursor pools [19], and shows positive results in various genotoxicity tests [18]. Despite a great number of investigations over the past 50 years, the MOA of these compounds is not well understood. The cytotoxic effect of maltol can be explained by its pro-oxidant properties; the maltol/metal complex generates reactive oxygen species (ROS) causing the production of hydroxyl radicals and leading to the formation of DNA base adducts [20]. However, no ROS-related DNA adducts were detected in the present analysis. Sodium chloride increased the incidence of MN cells at extremely high concentrations (c.a. 128 mM). Hyperosmotic medium can cause chromosomal aberrations in CHO cells, mutations at the TK locus in L5178Y mouse lymphoma cells, and at the HPRT locus in V79 cells [21]. However, the mechanisms by which abnormalities are induced in cells subjected to high osmotic pressure are unknown. Although the failure to detect DNA adducts with the non-carcinogens does not mean necessarily that DNA adducts were not formed, DNA adductome is the promising

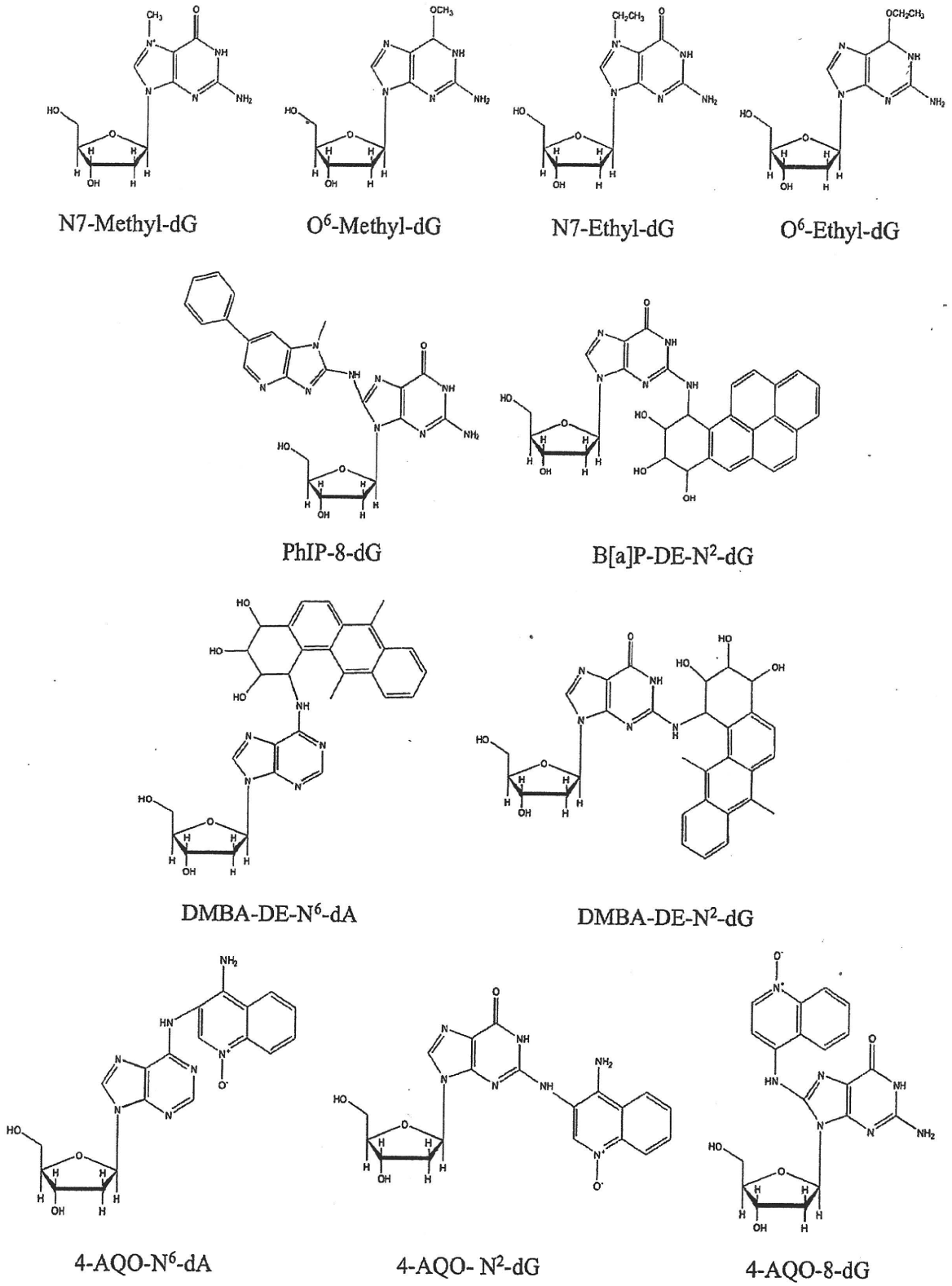

Fig. 2. Structures of DNA adducts estimated from their detected *m/z* values indicated in Table 2. The structures of DMBA-DE-N^6-dG and DMBA-DE-N^2-dG were estimated by the adduction pattern of other PAH compounds.

approach to distinguish false-positive genotoxic compounds from MN-positive compounds. The reliability of this approach will be improved more if the sensitivity of LC/MS/MS equipment is increased and the adductome protocol is more sophisticated.

In summary, with the conditions in which the test compounds significantly increased the frequency of MN cells, only carcinogens (groups A and B) yielded adduct peaks as expected (Table 2 and Fig. 3). The advantages of this adductome approach are as follows: (1) multiple types of DNA adducts can be detected comprehen-

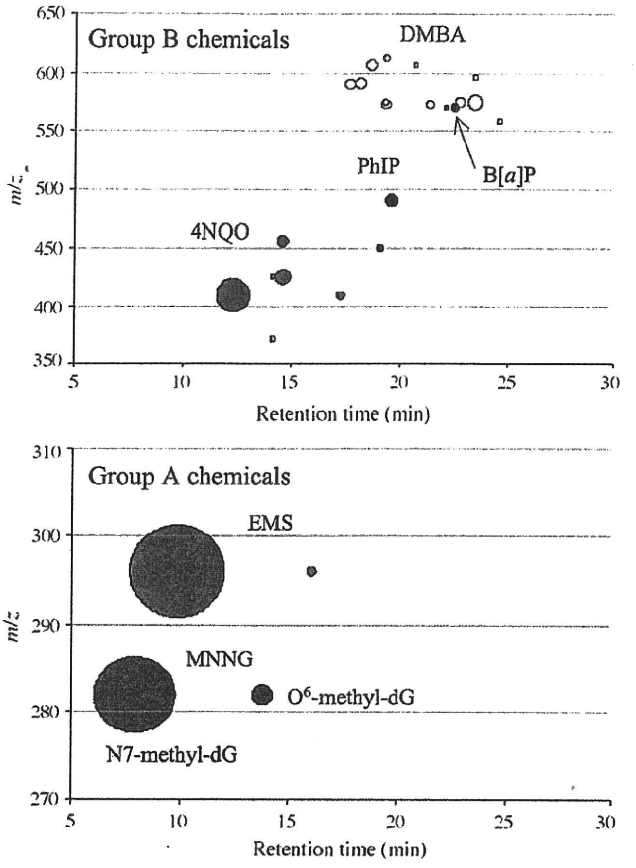

Fig. 3. DNA adductome maps of MN test positive carcinogens. CHL/IU cells were treated with Group A chemicals (carcinogens causing DNA alkylation) or Group B chemicals (carcinogens producing bulky DNA adducts), and the extracted DNA was digested by the MCN/SPD method (MNNG, EMS, B[*a*]P, DMBA) or nuclease P1 method (4-NQO and PhIP). The size of each bubble represents the "normalized peak area" shown in Table 2. Group A chemicals: EMS, pink; MNNG, brown. Group B chemicals: PhIP, blue; B[*a*]P, red; DMBA, yellow; 4-NQO, green. (For interpretation of the references to colour in this figure legend, the reader is referred to the web version of this article.)

sively, (2) the structures of the detected adducts can be identified from their *m/z* and their analytical standards, and (3) various experimental designs can be applied to both *in vitro* and *in vivo* samples. These experimental features resolve some limitations of the existing methods for analyzing DNA adduct formation.

This study is a pilot experiment to confirm the usefulness of the adductome approach to detect DNA adduct s produced by the compounds showing positive results in the MN test with different MOA. This approach enables detection of various types of DNA adducts formed by typical carcinogens, and does not enable detection of any adducts for non-carcinogens. We conclude that the adductome approach would be applicable to assess the DNA-damaging capability of many types of *in vitro* MN test-positive compounds, and also be useful for understanding MOA of the test compounds.

Conflicts of interest

The authors have no conflicts of interest to declare.

Acknowledgements

This research was performed as a cooperative research project among three institutions, Mitsubishi Tanabe Pharma Corporation, Kyoto University, and Osaka Prefecture University, which was supported by a fund from Mitsubishi Tanabe Pharma Corporation.

Appendix A. Supplementary data

Supplementary data associated with this article can be found, in the online version, at doi:10.1016/j.mrgentox.2010.11.012.

References

[1] D. Kirkland, M. Aardema, L. Henderson, L. Müller, Evaluation of the ability of a battery of 3 *in vitro* genotoxicity tests to descriminate rodent carcinogens and non-carcinogens. I. Sensitivity, specificity and relative predictivity, Mutat. Res. 584 (2005) 1–256.
[2] G.M. Williams, J. Whysner, Epigenetic carcinogens: evaluation and risk assessment, Exp. Toxicol. Pathol. 48 (1996) 189–195.
[3] D.H. Phillips, P.B. Farmer, F.A. Beland, R.G. Nath, M.C. Poirier, M.V. Reddy, K.W. Turteltaub, Methods of DNA adduct determination and their application to testing compounds for genotoxicity, Environ. Mol. Mutagen. 25 (2000) 222–233.
[4] R.A. Kanaly, T. Hanaoka, H. Sugimura, H. Toda, S. Matsui, T. Matsuda, Development of the adductome approach to detect DNA damage in humans, Antioxid. Redox Signal. 8 (2006) 993–1001.
[5] Y. Yang, D. Mikolic, S.M. Swanson, R.B. van Breeman, Quantitative determination of N^7-methyldeoxyguanosine and O^6-methyldeoxyguanosine in DNA by LC–UV–MS–MS, Anal. Chem. 74 (2002) 5376–5382.
[6] D.T. Beranek, Distribution of methyl and ethyl adducts following alkylation with monofunctional alkylating agents, Mutat. Res. 231 (1990) 11–30.
[7] P.D. Lowley, C.J. Thatcher, Methylation of deoxyribonucleic acid in cultured mammalian cells by *N*-methyl-*N'*-nitro-*N*-nitrosoguanidine, Biochem. J. 116 (1970) 693–707.
[8] D. Lin, K.R. Kaderlik, R.J. Turesky, D.W. Miller, J.O. Lay Jr., F.F. Kadlubar, Identification of *N*-(deoxyguanosin-8-yl)-2-amino-1-methyl-6-phenylimidazo[4,5-b]pyridine as the major adduct Formed by the food-borne carcinogen, 2-amino-1-methyl-6-phenylimidazo[4,5-b]pyridine, with DNA, Chem. Res. Toxicol. 5 (1992) 691–697.
[9] Q. Ruan, H.H. Kim, H. Jiang, T.M. Penning, R.G. Harvey, I.A. Blair, Quantification of benzo[a]pyrene diol epoxide DNA-adducts by stable isotope dilution liquid chromatography/tandem mass spectrometry, Rapid Commun. Mass Spectrom. 20 (2006) 1369–1380.
[11] K.W. Singletary, H.M. Parker, J.A. Milner, Identification and *in vivo* formation of ^{32}P-postlabeled rat mammary DMBA-DNA adducts, Carcinogenesis 11 (1990) 1959–1963.
[12] S. Galiègue-Zoutina, B. Bailleul, M. Loucheux-Lefevre, Adducts from *in vivo* auction of the carcinogen 4-hydroxyaminoquinoline 1-oxide in rats and from *in vitro* reaction of 4-acetoxyaminoquinoline 1-oxide with DNA and polynucleotides, Cancer Res. 45 (1985) 520–525.
[13] B. Bailleul, S. Galiègue, M. Loucheux-Lefebre, Adducts from the Reaction of O, O'-diacetyl or o-acetyl derivatives of the carcinogen 4-hydroxyaminoquinoline 1-oxide with purine nucleosides, Cancer Res. 41 (1981) 4559–4565.
[14] B. Bailleul, S. Galiègue-Zoutina, B. Perly, M. Loucheux-Lefebre, Structural identification of the purine ring-opened form of *N*-(deoxyguanosine-8yl)-4-aminoquinoline 1-oxide, Carcinogenesis 6 (1985) 319–332.
[15] S. Galiègue-Zoutina, B. Bailleul, Y. Ginot, B. Perly, P. Vigny, M. Loucheux-Lefebre, N^2-guanyl and N^6-adenyl arylation of chicken erythrocyte DNA by the ultimate carcinogen of 4-nitroquinoline 1-oxide, Cancer Res. 46 (1986) 1858–1863.
[16] Y. Arima, C. Nishigori, T. Takeuchi, S. Oka, K. Morimoto, A. Utani, Y. Miyachi, 4-nitroquinoline 1-oxide forms 8-hydroxydeoxyguanosine in human fibroblasts through reactive oxygen species, Toxicol. Sci. 91 (2006) 382–392.
[17] T. Hofer, C. Badouard, E. Bajak, J. Ravanat, Å. Mattsson, I.A. Cotgreave, Hydrogen peroxide causes greater oxidation in cellular RNA than DNA, Biol. Chem. 386 (1995) 333–337.
[18] H.S. Rosenkranz, F.K. Ennever, Evaluation of the genotoxicity of theobromine and caffeine, Food Chem. Toxicol. 25 (1987) 247–251.
[19] W.U. Müller, T. Bauch, A. Wojcik, W. Böcker, C. Streffer, Comet assay studies indicate that caffeine-mediated increase in radiation risk of embryos is due to inhibition of DNA repair, Mutagenesis 11 (1996) 57–60.
[20] K. Murakami, K. Ishida, K. Watanabe, R. Tsubouchi, M. Haneda, M. Yoshino, Prooxidant action of maltol: role of transition metals in the generation of reactive oxygen species and enhanced formation of 8-hydroxy-2'-deoxyguanosine formation in DNA, Biometals 19 (2006) 253–257.
[21] S.M. Galloway, D.A. Deasy, C.L. Bean, A.R. Kraynak, M.J. Armstrong, M.O. Bradley, Effects of high osmotic strength on chromosome aberrations, sister-chromatid exchanges and DNA strand breaks, and the relation to toxicity, Mutat. Res. 189 (1987) 15–25.

J Artif Organs
DOI 10.1007/s10047-011-0568-6

ORIGINAL ARTICLE

Efficient transfection method using deacylated polyethylenimine-coated magnetic nanoparticles

Daisuke Kami · Shogo Takeda · Hatsune Makino · Masashi Toyoda · Yoko Itakura · Satoshi Gojo · Shunei Kyo · Akihiro Umezawa · Masatoshi Watanabe

Received: 6 October 2010 / Accepted: 31 March 2011

Abstract Low efficiencies of nonviral gene vectors, such as transfection reagent, limit their utility in gene therapy. To overcome this disadvantage, we report on the preparation and properties of magnetic nanoparticles [diameter (d) = 121.32 ± 27.36 nm] positively charged by cationic polymer deacylated polyethylenimine (PEI max), which boosts gene delivery efficiency compare with polyethylenimine (PEI), and their use for the forced expression of plasmid delivery by application of a magnetic field. Magnetic nanoparticles were coated with PEI max, which enabled their electrostatic interaction with negatively charged molecules such as plasmid. We successfully transfected 81.1 ± 4.0% of the cells using PEI max-coated magnetic nanoparticles (PEI max-nanoparticles). Along with their superior properties as a DNA delivery vehicle, PEI max-nanoparticles offer to deliver various DNA formulations in addition to traditional methods. Furthermore, efficiency of the gene transfer was not inhibited in the presence of serum in the cells. PEI max-nanoparticles may be a promising gene carrier that has high transfection efficiency as well as low cytotoxicity.

Keywords Deacylated polyethylenimine · Magnetic nanoparticle · Efficient nonviral transfection method

D. Kami
Innovative Integration between Medicine and Engineering Based on Information Communications Technology, Yokohama National University Global COE Program, Yokohama, Japan
e-mail: dkami@tmig.or.jp

S. Takeda · M. Watanabe (✉)
Laboratory for Medical Engineering, Division of Materials and Chemical Engineering, Yokohama National University, 79-1 Tokiwadai, Hodogaya-ku, Yokohama 240-8501, Japan
e-mail: mawata@ynu.ac.jp

D. Kami · H. Makino · M. Toyoda · A. Umezawa
Department of Reproductive Biology, National Institute for Child Health and Development, Tokyo, Japan

D. Kami · M. Toyoda (✉) · Y. Itakura · S. Gojo
Vascular Medicine, Research Team for Geriatric Medicine, Tokyo Metropolitan Institute of Gerontology, 35-2 Sakae-cho, Itabashi-ku, Tokyo 173-0015, Japan
e-mail: mtoyoda@tmig.or.jp

S. Gojo · S. Kyo
Division of Therapeutic Strategy for Heart Failure, Department of Cardio-Thoracic Surgery, The University of Tokyo, Tokyo, Japan

Introduction

Nanotechnologies that allow the nondisruptive introduction of carriers in vivo have wide potential for gene and therapeutic delivery systems [1–4]. Extremely small particles have been successfully introduced into living cells without any further modification to enhance endocytic internalization, such as for cationic help. The cells containing the internalized nanoparticles continued to thrive, indicating that the particles have no inhibitory effect on mitosis. Therefore, iron oxide magnetic nanoparticles have played an important role as magnetic resonance imaging contrast agents [5, 6], and cytotoxicity of this nanoparticle was none (or low) [7, 8]. Thereby, the functionalized iron oxide magnetic nanoparticles are expected to be useful as a new gene delivery tool [3].

Cationic polymer polyethylenimine (linear, MW 25,000) (PEI) is known as the transfection reagent in molecular biology [9], and the dispersant in nanotechnology [10]. PEI are configured to form the positively charged complex with DNA, which binds to anionic cell surface residues and

Journal : Large 10047 | Dispatch : 18-4-2011 | Pages : 8
Article No. : 568 | LE | TYPESET
MS Code : JAO-D-10-00057 | CP | DISK

enter the cell via endocytosis [9, 11], keeping the dispersed state in the solution [10]. However, PEI containing residual *N*-acyl groups is a disadvantage for transfection efficiency. Also, the deacylated PEI (PEI max) for transfection reagent was reported, showing an increase in optimal transfection efficiency of 21-fold in comparison with PEI [12].

The transfection method using magnetic nanoparticles utilizes a magnetic force to deliver DNA into target cells. Therefore, the plasmid is first associated with magnetic nanoparticles. Then, the application of a magnetic force drives the plasmid–nanoparticle complexes toward and into the target cells, where the cargo is released (Fig. 1a) [13–16]. The magnetic nanoparticles are also coated with biological polymers, such as PEI, to allow plasmid loading (Fig. 1b). The binding of the negatively charged plasmid to the positively charged PEI max-coated magnetic nanoparticles (PEI max-nanoparticles) occurs relatively quickly. After complex formation, the loaded nanoparticles are incubated together with the target cells on a magnet plate. Owing to the magnetic force, the iron particles are rapidly drawn toward the surface of the cell membrane. Cellular uptake occurs by either endocytosis or pinocytosis [17]. Once delivered to the target cells, the plasmid is released into the cytoplasm [17, 18]. The magnetic nanoparticles accumulate in endosomes and/or vacuoles [18]. Over time, the nanoparticles are degraded and the iron enters normal iron metabolism [19]. An influence of magnetic nanoparticles on cellular functions has not been reported yet. However, in most cases, the increased iron concentration in culture media does not lead to cytotoxic effects [7].

In this study, we coated the transfection reagent, PEI max, on the surface of magnetic nanoparticles and applied a gene vector using PEI max-nanoparticles for a highly efficient transfection method. Our results indicate a high level of expression of the transfected gene in living cells using the plasmid-conjugated PEI max-nanoparticles.

Materials and methods

Materials

Magnetic nanoparticles (γ-Fe_2O_3, $d = 70$ nm) were purchased from CIK NanoTek. PEI max linear (MW 25,000) was purchased from Polysciences Inc. FuGENE HD was purchased from Roche Diagnostics. Deionized water was purchased from Gibco. Magnetic sheet (160 mT), and neodymium magnet (130 mT) was purchased from Magna Co. Ltd.

Preparation of the PEI max-nanoparticles

The magnetic nanoparticles (1.0 g) were dissolved in 30 ml of PEI max solution (1.6 mg PEI max/ml). The mixture was sonicated for 2 min (40 W) on ice, and 20 ml of deionized water was added (final concentration 1.0 mg PEI max/ml). The ferrofluid was centrifuged at 4,100×*g* for 5 min. The supernatant fluids were harvested and transferred into a fresh tube. This fluid was washed twice by deionized water and resolved into an equal volume of the PEI max solution (1.0 mg PEI max/ml). Magnetic

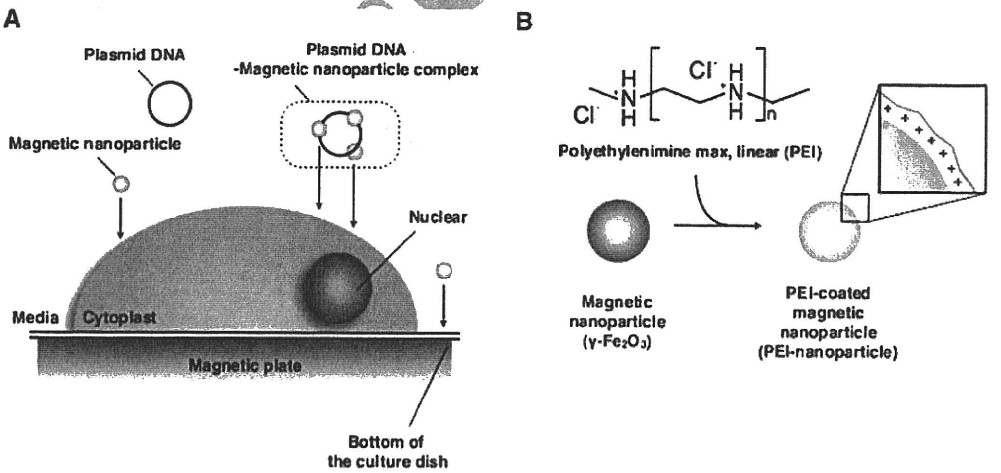

Fig. 1 Nanoparticle transfection method and cationic coating: **a** Plasmid-conjugated magnetic nanoparticles moved to the cell surface on the magnetic sheet upon application of magnetic force. Then, the magnetic force drove this complex toward and into the target cells. **b** Magnetic nanoparticles (γ-Fe_2O_3, $d = 70$ nm) (CIK NanoTek Inc.) were coated with deacylated polyethylenimine (PEI) max linear (MW 25,000) (Polysciences Inc.), known as a dispersive agent, and transfection reagents. The surface of the PEI max-nanoparticle was positively charged. Nanoparticles and plasmid formed complexes by ionic interaction of the negatively charged plasmid and the positively charged surface of the PEI max-nanoparticle

Journal : Large 10047 | Dispatch : 18-4-2011 | Pages : 8
Article No. : 568 | LE | TYPESET
MS Code : JAO-D-10-00057 | CP | DISK

nanoparticles in this fluid were coated with PEI max and dispersed in PEI max solution or deionized water.

Measurement of PEI max-nanoparticle size and ζ-potential

The size of the PEI max-nanoparticles was measured with a laser light-scattering method using a fiberoptics particle analyzer (FPAR-1000, Otsuka Electronics). The measurement was performed in triplicate, and median size and range of size distribution were obtained. The ζ-potential of the PEI max-nanoparticles was determined with electrophoretic light-scattering spectrophotometer (ELSZ-2, Otsuka Electronics).

Charge characteristics of PEI max-nanoparticle

PEI max-nanoparticle (100 μg) and each weight of plasmid (2,000, 1,000, 750, 500, 375, 250, 188 ng) were mixed in deionized water or PEI max solution (1 mg/ml). Each solution were reacted for 1 h at room temperature.

Plasmid DNA was bound to PEI max-nanoparticles

Plasmid DNA (5 μg) was reacted with various weights of PEI max-nanoparticles (0–1.8 mg/tube) in deionized water for 15 min at room temperature. Then, the reaction mixtures were centrifuged at 12,000×*g* for 15 min and were formed in a sol-like precipitation in the lower layer. The concentration of DNA in the upper layer (hyaline layer) was determined by NanoDrop 1000 spectrophotometer (Thermo Scientific). The relative concentration of plasmid DNA treated without PEI max-nanoparticles was regarded as 100%.

Cell culture

P19CL6 cells (CL6 cells) from a mouse embryonic carcinoma cell line were grown on 100-mm dishes (Becton-Dickinson) in alpha-minimum essentioal medium (MEM) (Nacalai Tesque) supplemented with 10% fetal bovine serum (FBS) (JRH Bioscience Inc.), penicillin, and streptomycin (Gibco), and were maintained in a 5% carbon dioxide (CO_2) atmosphere at 37°C.

Transfection procedure using PEI max-nanoparticles

CL6 cells were seeded at 1×10^5 cells/well in six-well plates (Becton-Dickinson) 18 h before transfection. Immediately before transfection, cells were rinsed and supplemented with fresh culture medium (1 ml). The PEI max-nanoparticles (in 1 mg PEI max/ml solution) were mixed with 2.0 μg of the plasmid [pCAGGS–enhanced green fluorescent protein (EGFP), the modified pCAGGS expression vector [20], weight ratio PEI max:plasmid = 3:1] and incubated in the deionized water at final volume of 50 μl at room temperature for 15 min. The complexes were added to the CL6 cells on a magnetic sheet various times (0, 0.5, 1, 4, and 24 h). Forty-eight hours after transfection, CL6 cells were evaluated; 1 mg/ml of PEI max solution was used as a positive control.

Quantitative real-time reverse transcriptional (RT)-PCR

Total RNAs from CL6 cells were extracted using ISOGEN (Nippon Gene). To perform quantitative real-time polymerase chain reaction (PCR) assay, total RNA (1 μg) was reverse-transcribed using random hexamer and the PrimeScript RT reagent kit (TaKaRa). Quantitative real-time reverse transcriptional (RT)-PCR was performed on LineGene (BioFlux), using 100 ng of complementary DNA (cDNA) in 25-μl reaction volumes with 10 nmol/l EGFP primer and 12.5 μl of SYBR Premix Ex Taq (TaKaRa). PCR primers for the gene of EGFP and *Gapdh* were designed to amplify each cDNA using the sense primer (5′-CCGA CCACATGAAGCAGCAC-3′) and the reverse primer (5′-CTTCAGCTCGATGCGGTTCAC-3′) for the EGFP, and the sense primer (5′-TGCGACTTCAACAGCAACTC-3′) and the reverse primer (5′-CTTGCTCAGTGTCCTTGC TG-3′) for the *Gapdh*. Calculations were automatically performed by fluorescent quantitative detection system software (BioFlux).

Nanoparticle cytotoxicity

Alamar Blue [21] was used to measure cell proliferation and metabolic activity as an oxidation-reduction indicator. After 48 h of PEI max or PEI max-nanoparticle exposure, 900 μl of medium from each condition was transferred into a 24-well flat-bottomed plate. One hundred microliters of Alamar Blue (AbD Serotec) was added to each well, and the well plate was incubated for 3 h at 37°C. Fluorescence was measured at 570/600 nm in a Viento multispectrophotometer reader (Dainippon Pharmaceutical). The relative absorbance of CL6 cells without any treatment is regarded as 100% (it is indicated as a percent control in Fig. 4c).

Flow cytometric analysis

To count the numbers of EGFP-positive cells using PEI max-nanoparticles (0.8 μg/well in a six-well plate) on a magnetic sheet for 4 h (PEI max alone as a positive control), a Cytomics FC500 (Beckman Coulter Inc.) was used, and data were analyzed with FlowJo Ver.7 (Tree Star Inc.). Each sample was compared with negative control cells (without treatment).

Journal : Large 10047 | Dispatch : 18-4-2011 | Pages : 8
Article No. : 568 | LE | TYPESET
MS Code : JAO-D-10-00057 | CP | DISK

Statistical analysis

Results, shown as the mean ± standard error (SE), were compared by analysis of variance (ANOVA) followed by Scheffe test (http://chiryo.phar.nagoya-cu.ac.jp/javastat/JavaStat-j.htm), with $P < 0.05$ considered significant.

Results

Characterization of PEI max-nanoparticles

Magnetic nanoparticles were well coated with PEI max and were highly dispersed in PEI max solution (1 mg/ml) or deionized water. Secondary size of the PEI max-nanoparticles was approximately 121.32 ± 27.36 nm (Fig. 2A). To evaluate stability in PEI max solution (1 mg/ml) or deionized water, we measured the ζ-potential of PEI max-nanoparticles, which was +45.53 mV in PEI max solution and +30.05 mV in deionized water. The PEI max-nanoparticles were aggregated by magnetic force (Fig. 2Ba) and quickly redispersed by vortex (Fig. 2Bb). Time-lapse photography (30 s/s) shows that magnetic nanoparticles were gradually removed at the site of the neodymium magnet (right side of the tube) for 2 h (magnetic nanoparticles for transfection: http://www.youtube.com/watch?v=Hyjfc4moHK4). These nanoparticles in PEI max solution were not aggregated without magnetic force. To avoid aggregation of plasmid-attached PEI max-nanoparticle caused by charge neutralization, it was necessary that their weight ratio was approximately 1:400 (Fig. 2C). In general, 1–2 μg of plasmid per well was mixed with the transfection reagent such, as PEI max, and FuGENE HD into six-well plates. However, too much (400–800 μg of nanoparticle per well) caused inhibition of transfection (described later). To solve the problem, we decided to use in 1 mg/ml of PEI max solution as a solvent. As a result, each concentration of the plasmid did not aggregate with PEI max-nanoparticle (Fig. 2Bb). To evaluate whether the plasmid DNA was attached to PEI max-nanoparticles in deionized water, we reacted PEI max-nanoparticles with plasmid DNA for 15 min at room temperature. Measuring the concentration of plasmid DNA in the upper layer (hyaline layer), the weight of PEI max-nanoparticles was reduced in a dependent manner (Fig. 2D).

Transfection efficiency using PEI max-nanoparticles and magnetic sheet, and viability of the CL6 cells treated with PEI max-nanoparticles

CL6 cells were transfected with pCAGGS-EGFP and PEI max alone as a positive control (Fig. 3a) and pCAGGS-EGFP and PEI max-nanoparticles (Fig. 3b) at 48 h after transfection. Many EGFP-positive cells were observed among CL6 cells transfected with PEI max-nanoparticles compared with those transfected with PEI max. To evaluate the optimum condition of transfection using PEI max-nanoparticles, quantitative real-time RT-PCR was performed at 48 h after transfection. The optimum condition of transfection was a concentration of 0.8 μg/well (Fig. 4a) on a magnetic sheet for 4 h (Fig. 4b). *EGFP* gene expression level was reduced under transfection of excess magnetic nanoparticles (7.5 μg/well) (Fig. 4a) and prolonged time on the magnetic sheet (24 h) (Fig. 4b). EGFP expression in CL6 cells transfected with PEI max-nanoparticles was increased approximately two to four-fold compared with those transfected with PEI max. The viability of CL6 cells treated with PEI max-nanoparticles, as measured by Alamar Blue assay, did not differ between cells treated with/without PEI max alone (Fig. 4c).

Number of EGFP-positive cells by flow cytometric analysis

Forty-eight hours after transfection using PEI max alone or PEI max-nanoparticles, we examined the number of EGFP-positive cells (total 10,000 cells) by flow cytometric analysis. Compared with the negative control (untreated CL6 cells), 42.2 ± 8.5% of cells treated with PEI max alone (Fig. 5a), 81.1 ± 4.0% of cells treated with 0.8 μg of PEI max-nanoparticles per well on the magnetic sheet for 4 h (Fig. 5b), and 13.9 ± 1.1% of cells treated with FuGENE HD (Fig. 5c) expressed EGFP. The number of EGFP-positive cells was significantly increased (approximately twofold) using PEI max-nanoparticles.

Discussion

In this study, to express target gene with high efficiency and low cytotoxicity, we focused on PEI max and magnetic nanoparticles (γ-Fe_2O_3). Many researchers have reported various transfection methods using PEI and magnetic nanoparticles, such as γ-Fe_2O_3, and superparamagnetic iron oxide nanoparticle (used as magnetic resonance imaging contrast agents) (Table 1). However, these methods had a low transfection efficiency [14, 15], combined with virus (adenovirus, or retrovirus) [15], and high cytotoxicity (low cell viability) [13] and may therefore have little effectiveness for clinical use.

The expression level of the *EGFP* gene was reduced under transfection of excess magnetic nanoparticles (7.5 μg/well) (Fig. 4a). This result may indicate that a high concentration of PEI max-nanoparticles formed the large agglutinate complexes with plasmid DNAs [22, 23]

Journal : Large 10047 | Dispatch : 18-4-2011 | Pages : 8
Article No. : 568 | LE | TYPESET
MS Code : JAO-D-10-00057 | CP | DISK

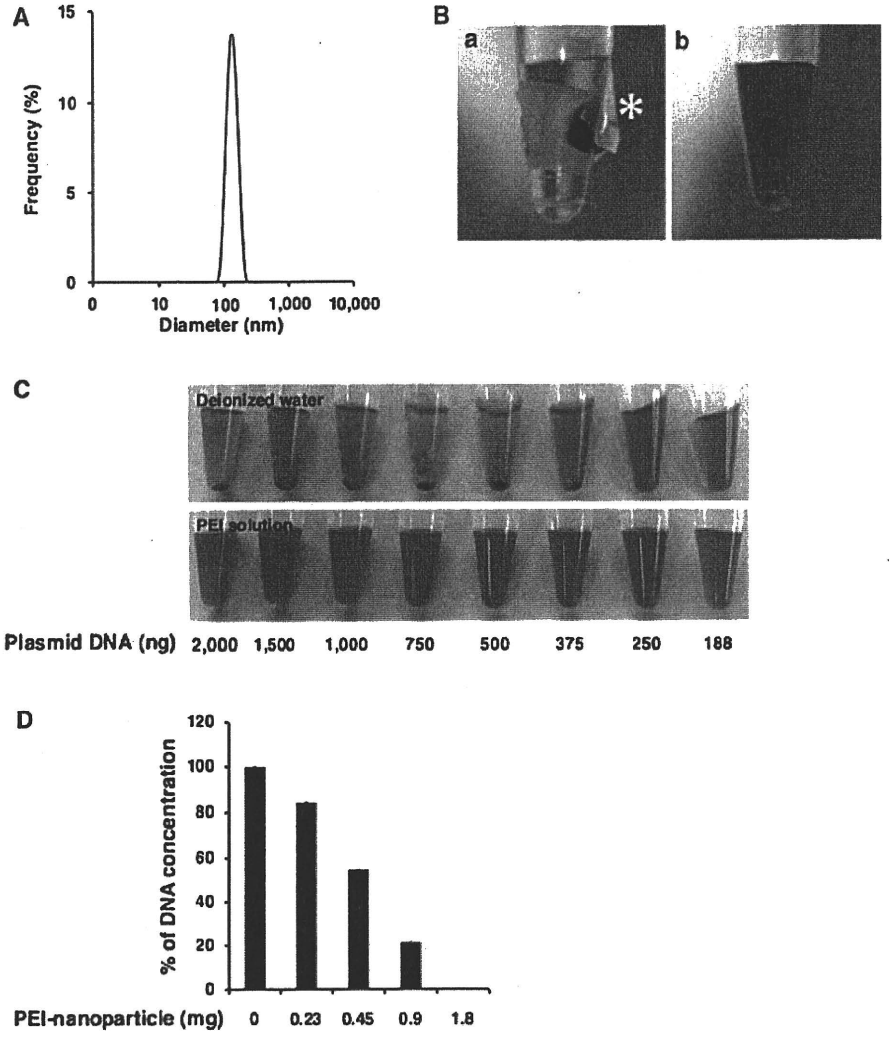

Fig. 2 Characteristics of the deacylated polyethylenimine (PEI max)-nanoparticle: **A** The size of the PEI max-nanoparticles was measured with a laser light-scattering method using a fiberoptics particle analyzer (FPAR-1000, Otsuka Electronics, Osaka, Japan) at 37°C. Secondary particle size of the PEI max-nanoparticles was approximately 121.32 ± 27.36 nm. **B** PEI max-nanoparticles were induced to aggregate by a magnet (*a*) and were then dispersed (*b*). *Asterisk* indicates column-shaped neodymium magnet. **C** Cationic PEI max-nanoparticles (100 μg per tube) in deionized water or PEI max solution (1 mg/ml) were reacted with anionic plasmid [pCAGGS–enhanced green fluorescent protein (EGFP)] by an ionic bond. PEI max-nanoparticles in deionized water and plasmid aggregated more easily than that in PEI max solution and plasmid. **D** To evaluate whether plasmid DNA attached to PEI max-nanoparticles in deionized water, PEI max-nanoparticles were reacted with plasmid DNA for 15 min at room temperature. Measuring the concentration of plasmid DNA in the upper layer (hyaline layer), the weight of PEI max-nanoparticles was reduced in a dependent manner

because PEI max-nanoparticle and plasmid DNA complexes are taken in by endocytosis. Thus, it might be difficult to take the large complexes into the cytoplasm by endocytosis. Furthermore, the expression level of the *EGFP* gene was also reduced under transfection during a prolonged time on the magnetic sheet (24 h) (Fig. 4b). This result may demonstrate a causal relationship between the cell division cycle and time on the magnetic sheet. Plasmid DNAs in the cytoplasm were transported into the nucleus when the nuclear membrane disappeared on cell division [24]. Thus, plasmid DNAs and magnetic nanoparticle complexes might not be transported into the nucleus because they are drawn to the bottom of the cell by magnetic force.

We succeeded in producing PEI max-nanoparticles that enabled P19CL6 cells, which is derived from embryonic carcinoma transfected on a magnetic sheet. In addition, this method resulted in a highly efficient gene transduction compared with that of conventional transfection methods (Fig. 5a, c). This transfection method using PEI max-nanoparticles is a relatively low-cost and quick method of introducing plasmid into target cells with increased

Journal : Large 10047 Dispatch : 18-4-2011 Pages : 8
Article No. : 568 LE TYPESET
MS Code : JAO-D-10-00057 CP DISK

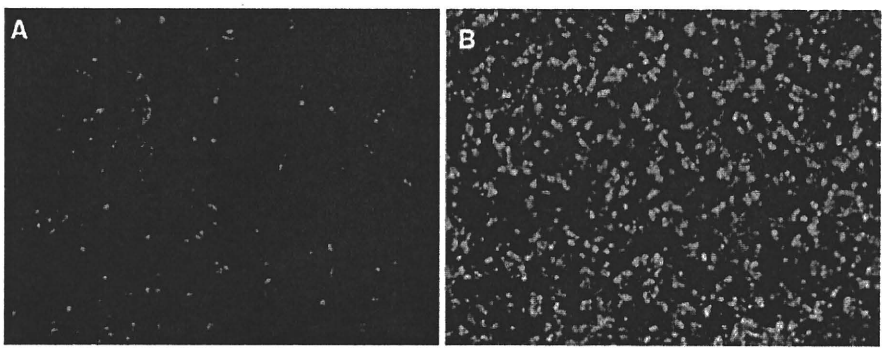

Fig. 3 Enhanced green fluorescent protein (EGFP) expression in CL6 cells using deacylated polyethylenimine (PEI max)-nanoparticle and magnetic field. Phase-contrast fluorescent micrograph of CL6 cells were transfected with pCAGGS-EGFP and PEI max as a control (**a**) and PEI max-nanoparticles (**b**). The numbers of EGFP-positive cells were further increased by PEI max-nanoparticles

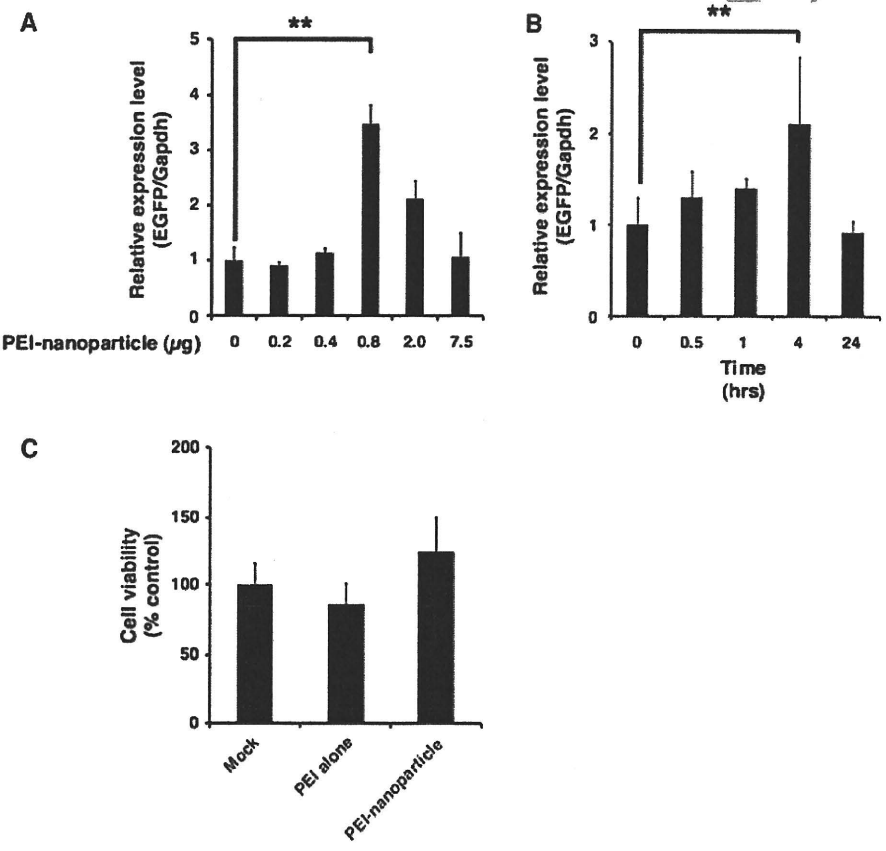

Fig. 4 Optimum condition for transfection of the deacylated polyethylenimine (PEI max)-nanoparticle. To optimize the transfection method, we examined PEI max-nanoparticles in terms of volume (**a**) and time (**b**) on the magnetic sheet. These results were evaluated by quantitative real-time reverse transcriptional polymerase chain reaction (RT-PCR). The expression level of the CL6 cells treated with PEI max alone is regarded as 1. The optimal conditions for transfection using PEI max-nanoparticles were when the CL6 cells were treated with 0.8 μg of PEI max-nanoparticles and 2.0 μg of pCAGGS-EGFP for 4 h on the magnetic sheet. The *double asterisks* indicate a significant difference ($P < 0.05$). Cytotoxicities of PEI max and PEI max-nanoparticles were evaluated by Alamar Blue assay (**c**). After 48 h of PEI max or PEI max-nanoparticle exposure, there were no significant differences in cell viability between CL6 cells treated with PEI max and those with PEI max-nanoparticles. *Mock* the CL6 cells treated without any treatment as a negative control. *PEI max alone* the CL6 cells treated with PEI max. *PEI max-nanoparticles* the CL6 cells treated with PEI max-nanoparticles (0.8 μg) for 4 h on the magnetic sheet. The relative absorbance of untreated CL6 cells is regarded as 100%

Journal : Large 10047 | Dispatch : 18-4-2011 | Pages : 8
Article No. : 568 | ☐ LE | ☐ TYPESET
MS Code : JAO-D-10-00057 | ☑ CP | ☑ DISK

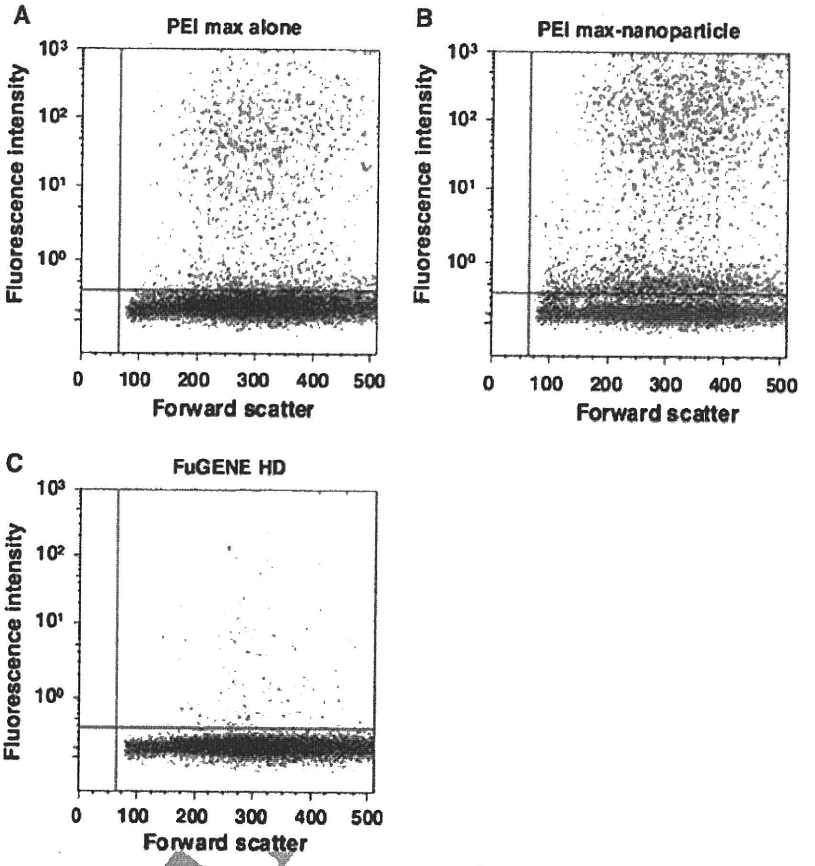

Fig. 5 Transfection efficiency of the deacylated polyethylenimine (PEI max)-nanoparticle. Comparison of scattering properties of the untreated CL6 cells (mock, *red dot*) and with PEI max alone (**a**, *blue dot*, 42.2 ± 8.5%), PEI max-nanoparticles (**b**, *blue dot*, 81.1 ± 4.0%), or FuGENE HD (**c**, *blue dot*, 13.9 ± 1.1%) by flow cytometry

Table 1 Comparison of transfection methods using the polyethylenimine and magnetic nanoparticles

Author	Year	Vector	Component	Cell	Transfection efficiency	Cell viability (% of control)	References
Kami	–	Plasmid	PEI max (MW 25k), MNP (γ-Fe2O3, 70 nm), MF (0.2 T)	P19CL6	80%[a]	100	This paper
Zhang	2010	Plasmid	Branched PEI (MW 25k), SPION (30 nm), MF (1.2 T)	NIH3T3	64%[a]	100	[14]
		siRNA	Branched PEI (MW 25k), SPION (30 nm), MF (1.2 T)	NIH3T3	77%[a]	100	
Kievit	2009	Plasmid	PEI (MW 25k), SPION (200 nm)	C6	90%[a]	10	[13]
		Plasmid	PEI (MW 25k), Chitosan, SPION (200 nm)	C6	45%[a]	100	
		Plasmid	PolyMag (commercial magnification reagent), MF (1.2 T)	C6	32%[a]	66	
Scherer	2002	Plasmid	PEI (MW 800k), SPION (200 nm), MF (1 T)	NIH3T3	5-fold[b]	–	[15]
		Adenovirus	PEI (MW 800k), SPION (200 nm), MF (1 T)	K562	100-fold[b]	–	
		Retrovirus	PEI (MW 800k), SPION (200 nm), MF (1 T)	NIH3T3	20%[a]	–	

Transfection efficiency indicates optimal transfection condition

PEI polyethylenimine, *PEI max* deacylated PEI, *MNP* magnetic nanoparticle, *SPION* superparamagnetic iron oxide nanoparticle, *MW* molecular weight, *MF* magnetic force, *T* tesla

[a] Flowcytometric analysis

[b] Luciferase activity assay

efficiency. Furthermore, a major advantage of this method is its tolerability among cells. Other methods might be limited either by possible cytotoxic effects of the lipidic transfection reagent (lipofection) or simply by the directly applied force on the cells (electroporation). In contrast, methods such as lipofection offer only a certain probability of hits between cargo and cells because of the three-dimensional motion of cells and transfection aggregates in a liquid suspension. Normally, transfection was inhibited by serum using transfection reagent [25]. However, this

Journal : Large 10047 Dispatch : 18-4-2011 Pages : 8
Article No. : 568 LE TYPESET
MS Code : JAO-D-10-00057 CP DISK

method can also be performed in the presence of serum, which is a further benefit. Additionally, synergistic effects on transfection efficiency can arise from the possible combination of PEI max and nanoparticles. This technology might be an alternative to the currently used viral and nonviral vectors in gene therapy and gene transfer [26].

Our results suggest that PEI max-nanoparticles offer the ability to deliver various DNA formulations in addition to the traditional methods. Furthermore, gene transfer efficiency was not inhibited in the presence of serum in the cells. PEI max-nanoparticles may be a promising gene carrier with high transfection efficiency and low cytotoxicity.

Acknowledgments We express our sincere thanks to Koichiro Nishino (Department of Reproductive Biology, National Institute for Child Health and Development) for pCAGGS-EGFP. This study was supported by a Grant-in-Aid for the Global COE Program, Science for Future Molecular Systems, for SS and TO from the Ministry of Education, Culture, Sports, Science and Technology, Japan (MEXT).

References

1. Kimura T, Iwai S, Moritan T, Nam K, Mutsuo S, Yoshizawa H, Okada M, Furuzono T, Fujisato T, Kishida A. Preparation of poly(vinyl alcohol)/DNA hydrogels via hydrogen bonds formed on ultra-high pressurization and controlled release of DNA from the hydrogels for gene delivery. J Artif Organs. 2007;10:104–8.
2. Moritake S, Taira S, Ichiyanagi Y, Morone N, Song SY, Hatanaka T, Yuasa S, Setou M. Functionalized nano-magnetic particles for an in vivo delivery system. J Nanosci Nanotechnol. 2007;7:937–44.
3. Tomitaka A, Koshi T, Hatsugai S, Yamada T, Takemura Y. Magnetic characterization of surface-coated magnetic nanoparticles for biomedical application. J Magn Magn Mater. 2010;323:1396–1403.
4. Yokoyama M. Drug targeting with nano-sized carrier systems. J Artif Organs. 2005;8:77–84.
5. Lauterbur PC, et al. Image formation by induced local interactions. Examples employing nuclear magnetic resonance. Clin Orthop Relat Res. 1973;1989:3–6.
6. Nakamura H, Ito N, Kotake F, Mizokami Y, Matsuoka T. Tumor-detecting capacity and clinical usefulness of SPIO-MRI in patients with hepatocellular carcinoma. J Gastroenterol. 2000;35:849–55.
7. Karlsson HL, Cronholm P, Gustafsson J, Moller L. Copper oxide nanoparticles are highly toxic: a comparison between metal oxide nanoparticles and carbon nanotubes. Chem Res Toxicol. 2008;21:1726–32.
8. Karlsson HL, Gustafsson J, Cronholm P, Moller L. Size-dependent toxicity of metal oxide particles–a comparison between nano- and micrometer size. Toxicol Lett. 2009;188:112–8.
9. Boussif O, Lezoualc'h F, Zanta MA, Mergny MD, Scherman D, Demeneix B, Behr JP. A versatile vector for gene and oligonucleotide transfer into cells in culture and in vivo: polyethylenimine. Proc Natl Acad Sci USA. 1995;92:7297–301.
10. Wang J, Gao L. Adsorption of polyethylenimine on nanosized zirconia particles in aqueous suspensions. J Colloid Interface Sci. 1999;216:436–9.
11. Vancha AR, Govindaraju S, Parsa KV, Jasti M, Gonzalez-Garcia M, Ballestero RP. Use of polyethyleneimine polymer in cell culture as attachment factor and lipofection enhancer. BMC Biotechnol. 2004;4:23.
12. Thomas M, Lu JJ, Ge Q, Zhang C, Chen J, Klibanov AM. Full deacylation of polyethylenimine dramatically boosts its gene delivery efficiency and specificity to mouse lung. Proc Natl Acad Sci USA. 2005;102:5679–84.
13. Kievit FM, Veiseh O, Bhattarai N, Fang C, Gunn JW, Lee D, Ellenbogen RG, Olson JM, Zhang M. PEI-PEG-chitosan copolymer coated iron oxide nanoparticles for safe gene delivery: synthesis, complexation, and transfection. Adv Funct Mater. 2009;19:2244–51.
14. Zhang H, Lee MY, Hogg MG, Dordick JS, Sharfstein ST. Gene delivery in three-dimensional cell cultures by superparamagnetic nanoparticles. ACS Nano. 2010;4:4733–43.
15. Scherer F, Anton M, Schillinger U, Henke J, Bergemann C, Kruger A, Gansbacher B, Plank C. Magnetofection: enhancing and targeting gene delivery by magnetic force in vitro and in vivo. Gene Ther. 2002;9:102–9.
16. Bertram J. MATra—magnet assisted transfection: combining nanotechnology and magnetic forces to improve intracellular delivery of nucleic acids. Curr Pharm Biotechnol. 2006;7:277–85.
17. Arsianti M, Lim M, Marquis CP, Amal R. Polyethylenimine based magnetic iron-oxide vector: the effect of vector component assembly on cellular entry mechanism, intracellular localization, and cellular viability. Biomacromolecules. 2010;11:2521–31.
18. Georgieva JV, Kalicharan D, Couraud PO, Romero IA, Weksler B, Hoekstra D, Zuhorn IS. Surface characteristics of nanoparticles determine their intracellular fate in and processing by human blood-brain barrier endothelial cells in vitro. Mol Ther. 2011;19:318–25.
19. Longmire M, Choyke PL, Kobayashi H. Clearance properties of nano-sized particles and molecules as imaging agents: considerations and caveats. Nanomedicine (Lond). 2008;3:703–17.
20. Niwa H, Yamamura K, Miyazaki J. Efficient selection for high-expression transfectants with a novel eukaryotic vector. Gene. 1991;108:193–9.
21. Nakayama GR, Caton MC, Nova MP, Parandoosh Z. Assessment of the Alamar blue assay for cellular growth and viability in vitro. J Immunol Methods. 1997;204:205–8.
22. Namgung R, Singha K, Yu MK, Jon S, Kim YS, Ahn Y, Park IK, Kim WJ. Hybrid superparamagnetic iron oxide nanoparticle-branched polyethylenimine magnetoplexes for gene transfection of vascular endothelial cells. Biomaterials. 2010;31:4204–13.
23. Song HP, Yang JY, Lo SL, Wang Y, Fan WM, Tang XS, Xue JM, Wang S. Gene transfer using self-assembled ternary complexes of cationic magnetic nanoparticles, plasmid DNA and cell-penetrating Tat peptide. Biomaterials. 2010;31:769–78.
24. Coonrod A, Li FQ, Horwitz M. On the mechanism of DNA transfection: efficient gene transfer without viruses. Gene Ther. 1997;4:1313–21.
25. Purow BW, Sundaresan TK, Burdick MJ, Kefas BA, Comeau LD, Hawkinson MP, Su Q, Kotliarov Y, Lee J, Zhang W, Fine HA. Notch-1 regulates transcription of the epidermal growth factor receptor through p53. Carcinogenesis. 2008;29:918–25.
26. Davis ME. Non-viral gene delivery systems. Curr Opin Biotechnol. 2002;13:128–31.

Journal : Large 10047 | Dispatch : 18-4-2011 | Pages : 8
Article No. : 568 | LE | TYPESET
MS Code : JAO-D-10-00057 | CP | DISK

Induction of Glandular Stomach Cancers in *Helicobacter pylori*-infected Mongolian Gerbils by 1-Nitrosoindole-3-acetonitrile

Satoshi Matsubara[1,2], Shinji Takasu[1], Tetsuya Tsukamoto[3], Michihiro Mutoh[1], Shuichi Masuda[4], Takashi Sugimura[1], Keiji Wakabayashi[1,4] and Yukari Totsuka[1,*]

[1]Cancer Prevention Basic Research Project, National Cancer Center Research Institute, 1-1, Tsukiji 5-chome, Chuo-ku, Tokyo 104-0045, Japan

[2]Food Research Department, Yakult Central Institute for Microbiological Research, 1796, Yaho, Kunitachi-shi, Tokyo 186-8650, Japan

[3]Department of Pathology and Matrix Biology, Mie University Graduate School of Medicine, 2-174 Edobashi, Tsu-shi, Mie 514-8507, Japan

[4]Department of Food and Nutritional Sciences, Graduate School of Nutritional and Environmental Sciences, University of Shizuoka, 52-1, Yada, Shizuoka 422-8526, Japan

*To whom correspondence should be addressed. Tel: +81-3-3542-2511; Fax: +81-3-3543-9305; Email:ytotsuka@ncc.go.jp

Key words: gastric cancer, *Helicobacter pylori*, Mongolian gerbil, 1-nitrosoindole-3-acetonitrile, indole-3-acetonitrile

Abbreviations: DMSO, dimethyl sulfoxide; *H. pylori*, *Helicobacter pylori*; H&E, hematoxylin and eosin; MG, Mongolian gerbil; MNNG, *N*-methyl-*N*'-nitro-*N*-nitrosoguanidine; MNU, *N*-methyl-*N*-nitrosourea; NIAN, 1-nitrosoindole-3-acetonitrile.

Appropriate category: Carcinogenesis

Abstract

Helicobacter pylori (*H. pylori*) infection and high intake of various traditional salt-preserved foods are regarded as risk factors for human gastric cancer. We previously reported that Chinese cabbage contains indole compounds, such as indole-3-acetonitrile, a mutagen precursor. 1-Nitrosoindole-3-acetonitrile (NIAN), formed by the treatment of indole-3-acetonitrile with nitrite under acidic conditions, shows direct-acting mutagenicity. In the present study, NIAN administration by gavage to Mongolian gerbils (MGs) at the dose of 100 mg/kg two times a week resulted in three adduct spots (1.6 adducts/10^8 nucleotides in total), detected in DNA samples from the glandular stomach by ^{32}P-postlabelling methods. Treatment with six consecutive doses of 100 mg/kg of NIAN, two times a week for three weeks, induced well- and moderately-differentiated glandular stomach adenocarcinomas in the MGs at the incidence of 31% under *H. pylori* infection at 54 - 104 weeks. Such lesions were not induced in MGs given broth alone, broth + NIAN or infection with *H. pylori* alone. Thus, endogenous carcinogens formed from nitrosation of indole compounds could

be critical risk factors for human gastric cancer development under the influence of *H. pylori* infection.

Introduction

Gastric cancer is the second most frequent cause of cancer death worldwide.[1] Although gastric cancer has become a relatively rare cancer in North America and most Northern and Western European countries, it remains common in East Asia, Eastern Europe, Russia and selected areas of Central and South America.[2] *Helicobacter pylori* (*H. pylori*) is a well-established major risk factor for gastric cancer,[3-5] and the prevalence of *H. pylori* infection in East Asia countries, including Japan and Korea is reported to be relatively high.[6, 7] In addition, the risk of gastric cancer is increased with a high intake of various traditional salt-preserved foods.[3] In fact, pickled vegetable consumption is reported to increase gastric cancer risk in Japan and Korea.[8-10] In Korea, kimchi, commonly prepared with Chinese cabbage or radish, is a traditional and popular food, which contains high levels of nitrate (median 1550 mg/kg).[11] Furthermore, Chinese cabbage is well known as a pickled

vegetable commonly consumed in Japan. Moreover, ingestion of nitrate, mainly from food, is suggested to correlate with mortality from gastric cancer.[12-14] Ingested nitrate is mainly converted to nitrite by bacteria in the oral cavity after secretion into saliva.[15] Carcinogenic *N*-nitroso compounds can be formed from nitrite and secondary amines under acidic conditions. Furthermore, direct-acting *N*-nitroso compounds, such as *N*-methyl-*N*'-nitro-*N*-nitrosoguanidine (MNNG)[16] and *N*-methyl-*N*-nitrosourea (MNU),[17] are known to induce cancer in the glandular stomach of experimental animals. Thus, it is suggested that *N*-nitroso compounds that are formed in the stomach under acidic conditions could be positively associated with the risk of gastric cancer. Nitric oxide, formed by nitric oxide synthase, is also reported to contribute to production of *N*-nitroso compounds.[18]

We have previously reported that treatments of various foodstuffs with nitrite under acidic conditions produce direct-acting mutagens towards *Salmonella* tester strains.[19, 20] Among those foodstuffs, Chinese cabbage is shown to contain three indole compounds, indole-3-acetonitrile,

4-methoxyindole-3-acetonitrile and 4-methoxyindole-3-aldehyde as mutagen precursors. 1-Nitrosoindole-3-acetonitrile (NIAN), an *N*-nitroso-substituted compound formed by treatment of indole-3-acetonitrile with nitrite under acidic conditions, is a direct-acting mutagen in *S. typhimurium* and Chinese hamster lung cells,[20-22] and it is confirmed to form DNA adducts and to induce DNA single-strand scission in the rat glandular stomach.[23, 24] Therefore, NIAN could play some role in gastric cancer development, as in the case of the well-known direct-acting mutagens, MNNG and MNU, in animal experiments.[16, 17, 25]

The Mongolian gerbil (MG) is reported to be susceptible to colonization by *H. pylori*, and *H. pylori* infection greatly enhances MNNG or MNU-induced gastric carcinogenesis in MGs.[26, 27] Therefore, the MG is considered to be a useful animal model for evaluating the gastric cancer risk of direct-acting *N*-nitroso compounds, with or without *H. pylori* infection.

Chinese cabbage, containing nitrate and indole compounds, is commonly consumed in East Asian countries, including Japan,

Korea and China, in which gastric cancer mortality is very high. In the present study, DNA adducts were detected with NIAN treatment in the glandular stomach of MGs, and the carcinogenicity of NIAN for gastric cancer *in vivo* was examined. The results clearly demonstrated that gastric cancer developed with a combination of NIAN administration and *H. pylori* infection in MGs. Possible involvement of indole compounds and nitrate derived from various foodstuffs, including Chinese cabbage, in gastric cancer development in humans is discussed.

Materials and Methods

Materials

Indole-3-acetonitrile was purchased from Tokyo Food Techno Co., Ltd. (Tokyo, Japan), sodium nitrite from Wako Pure Chemical Industries, Ltd. (Osaka, Japan), and ammonium sulfamate from Kanto Chemical Co., Inc. (Tokyo, Japan). Brucella broth was obtained from Becton Dickinson Co. (Cockeysville, MD, USA), and horse serum from Nippon Bio-Supply (Tokyo, Japan).

Preparation of NIAN

The chemical structure of NIAN is shown in Figure 1A. Indole-3-acetonitrile in 27 mM citrate-phosphate buffer (pH 3.0) was treated with 50 mM sodium nitrite for 1 hour at room temperature in the dark, as previously reported.[21] Nitrosation was stopped by addition of ammonium sulfamate at a final concentration of 50 mM. The reaction solution was filtered and the residue was washed with deionized water, then with n-hexane. The residual paste was dried and stored at -80°C until use. The preparation was >93% pure as judged by its UV absorbance on HPLC.

Bacterial culture

H. pylori (ATCC 43504; American Type Culture Collection, Manassas, VA) was cultured in brucella broth supplemented with 10% heat-inactivated horse serum for 24 hours at 37 °C under microaerobic conditions (5% O_2, 10% CO_2 and 85% N_2), as previously described.[28]

Animal treatment

Specific pathogen-free male, 6-week-old MGs (MGS/Sea, Kyudo,